

Comparing Geometrical Properties of Global Grids

A. Jon Kimerling, Kevin Sahr, Denis White, and Lian Song

ABSTRACT: Transforming raw observations into geometrically regular global grids is a fundamental data processing and storage problem underlying much of our global data analysis. The basic geometry of traditionally employed quadrilateral-based point or area grids, while well suited to array storage and matrix manipulation, may inherently hinder numerical and geostatistical modeling efforts. Several scientists have noted the superior performance of triangular point grids and associated triangular cells that can be aggregated into hexagonal surface tessellations, yet, no thorough evaluation of discrete global grid alternatives has been conducted. We present results from a global grid comparison study that focused on recursive tiling of polyhedral faces projected onto the globe. A set of evaluation criteria for global partitioning methods were developed. Of these, metrics for spheroidal surface area, compactness, and centerpoint spacing were found to be of particular importance. We present examples of these metrics applied to compare different recursive map projection-based and quadrilateral spherical partitionings. One map projection approach, the Icosahedral Snyder Equal Area (ISEA), shows particular promise due to its production of equal area triangular and hexagonal cells on the spheroid at all levels of recursive partitioning.

KEYWORDS: Global grids, spherical surface tessellations, global data models, distortion analysis

Introduction

A new era of high spatial and temporal resolution environmental data covering the entire globe is about to begin, ushered in by NASA's Earth Observation System (EOS) and other global data collection efforts. Examples are the 1 km AVHRR, land cover (Loveland et al. 1991), and digital elevation model (DEM) data sets compiled as part of the International Geosphere-Biosphere Program's Data and Information System (Eidenshink and Faundeen 1994; Hastings 1996). We should expect that earth scientists will accelerate their use of geographic information systems (GIS), numerical modeling approaches, and geostatistical methods, singly or in concert, to study global scale phenomena. Phenomena of varying time scales, such as climate change, deforestation, biodiversity loss, biogeochemical cycles, and transports/budgets in the atmosphere and oceans, are beginning to be studied as an interconnected global system. Such global analyses will require both spatial and temporal

integration of currently disparate data sets from a wide variety of data producers (Kahn 1995). Transforming the raw observations underlying global analyses into a global grid is a fundamental data processing and storage problem.

A global grid is a tessellation of the Earth into a geometrically regular set of cells, with associated cell centerpoints. A highly regular global grid would allow us to:

- Summarize and organize the multiple, non-uniformly spaced measurements over the globe;
- Calculate gradients faithfully (e.g., for budget calculations);
- Make comparisons of time-series of globally distributed data (e.g., for detecting climate changes);
- Make statistically meaningful regional comparisons of globally distributed data;
- Compare and combine data sets taken at different spatial resolutions, such as data from multiple satellite measurements and field verification data;
- Improve the operation of numerical models based on finite difference equations; and
- Document the precision as well as the location of spatial data on the globe.

Geometrical regularity is the challenge. Currently utilized "regular" global grids, such as the ETOPO5 5 minute DEM or the NASA Earth Radiation Budget Experiment (ERBE) 2.5° global modeling grid, cannot be extended to the entire Earth

A. Jon Kimerling is a professor of geography, Kevin Sahr is a research assistant, and Lian Song is a former graduate student research assistant in the Department of Geosciences, Oregon State University, Corvallis, OR 97331. Denis White is a geographer at the U.S. Environmental Protection Agency, Corvallis, OR 97333. Comments to A. Jon Kimerling at (541) 737-1225 or e-mail: <kimerlia@geo.orst.edu>.

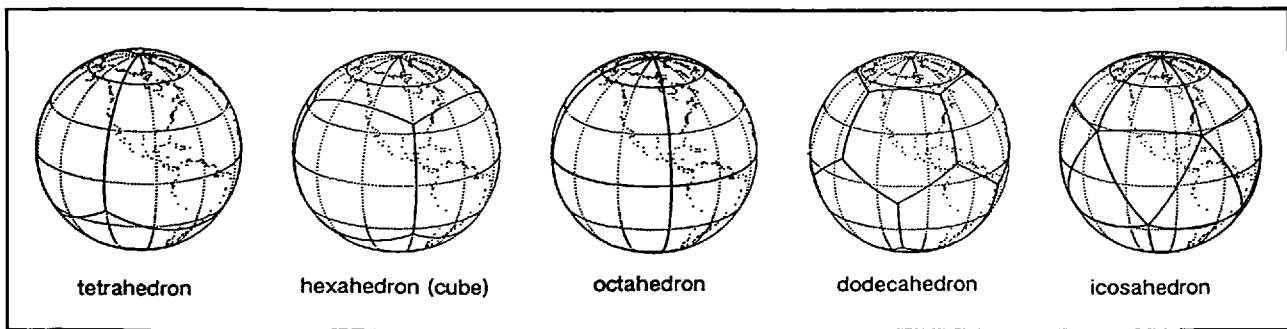


Figure 1. The spherical tessellations of the five regular polyhedra.

without losing regularity in both surface area and shape. Alternative approaches beg investigation. Subdividing the globe with total regularity of surface area and polygonal shape within the cells formed by the subdivision can be achieved only by projecting the faces of one of the five Platonic polyhedra onto the globe (Figure 1). Further partitioning of any face will produce unavoidable variations in surface area, shape, or both. Area partitioning is closely tied to the problem of uniformly placing a large number of points over the surface of a sphere, and optimizing the placement of points has challenged scientists working in fields as diverse as viral morphology, crystallography, and electrostatics (Saff and Kuijlaars 1997).

Equally important is the realization that the basic geometry of commonly employed quadrilateral point grids or surface tessellations, while well suited to array storage and matrix manipulation, may inherently hinder numerical and geostatistical modeling efforts. Scientists have noted the superior performance of triangular point grids and associated hexagonal surface tessellations for numerical analyses central to cellular automata (Wolfram 1986), percolation theory (Stauffer 1992), and self-avoiding walks (Slade 1994). Hexagonal tessellations are favored by influential statisticians involved with developing survey sample designs and geostatistical methods such as Kriging (Olea 1984). Additionally, mathematicians studying spherical point distributions note that the general geometric pattern for optimal configurations always is the same: large numbers of points “appear to arrange themselves according to a hexagonal pattern that is slightly perturbed in order to fit on the sphere” (Saff and Kuijlaars 1997).

It is clear that a thorough evaluation and comparison of alternative global grids is needed. In this article we present an evaluation approach centered on cell geometry and topology, as well as results from a global grid comparison study funded by the U.S. Environmental Protection Agency (White et al 1992; 1998). We begin by developing a

comprehensive list of grid evaluation criteria, along with metrics for many of the criteria. We next describe grid alternatives that are examples of basic approaches to tessellating the globe. Our comparison metrics are next applied to these grids, and the results of this analysis are presented in both maps and statistical summaries. We conclude by recommending a particular grid—the Icosahedral Snyder Equal Area (ISEA)—for global modeling efforts, and note several topics for further research.

Global Grid Comparison Criteria

Partitioning the globe into a global grid with prescribed fineness results in area or shape distortion, or both. Different partitioning approaches will introduce different magnitudes of these distortions. Therefore, it is necessary to have a set of ideal geometric/topologic properties and corresponding mathematical metrics for each of the properties to serve as comparison standards for alternative global grids. These properties of an ideal global grid are organized into the list of general evaluation criteria shown below. An early version of these criteria was formulated by Michael Goodchild (1994), and we refer to this list as the “Goodchild Criteria.”

1. Areal cells constitute a complete tiling of the globe, exhaustively covering the globe without overlapping.
2. Areal cells have equal areas. This minimizes the confounding effects of area variation in analysis, and provides equal probabilities for sampling designs.
3. Areal cells have the same topology. Ideally, this means that every cell has the same number of edges and vertices. This may not apply to grids whose cell boundaries are arbitrary curves.
4. Areal cells are the same shape. Exactly what this means is highly dependent on the nature of the specific grid. In the ideal case, each cell would be a regular spherical polygon, with edges consisting

of great circle arcs of lengths corresponding to those of every other cell.

5. Areal cells are compact. Because a single vector of values will be associated with all the points in a single areal cell, it is preferable that the actual values of all the points in the cell be as much alike as possible. Maximal compactness ensures that the points in a cell are as close to each other as possible, thus taking advantage of Tobler's first law of geography, which in this case is that the closer points are in space, the more likely they are to be alike.
6. Edges of cells are straight in a projection. Again, this assumes that the concept of edges has meaning for a particular grid (i.e., that the cell boundaries are not arbitrary curves). This criterion ensures the existence of a relatively convenient space for describing, visualizing, and working with grid cells.
7. The midpoint of the arc connecting two adjacent cell centers coincides with the midpoint of the edge between the two cells. This criterion has proved useful in calculating transport between cells using finite differences (Heikes and Randall 1995).
8. The points and areal cells of the various resolution grids which constitute the grid system form a hierarchy which displays a high degree of regularity. If a hierarchical structure exists, grid cells may be subdivided recursively, and a nested set of geometrically similar cells may be created from the set of smallest cells, reducing the burden of recalculation as the fineness of resolution changes. A hierarchical structure should also enable activities such as efficient computer implementation of the grid system and multi-resolution analysis using the grid system.
9. A single areal cell contains only one grid reference point, i.e., each reference point lies in a different areal cell.
10. Grid reference points are maximally central within areal cells. In conjunction with the last criterion, this optimally supports the common practice of using the point grid as an approximation to the area grid.
11. Grid reference points are equidistant from their neighbors.
12. Grid reference points and areal cells display regularities and other properties which allow them to be addressed in an efficient manner. The grid system should provide an addressing system that supports efficient algorithms for such common grid operations as determining cell and point neighbors, determining grid distances, and moving between grid resolutions.

13. The grid system has a simple relationship to the traditional latitude-longitude graticule. Since for the indefinite future most data will be georeferenced using the latitude-longitude graticule, efficient ways of transferring data to and from this system will be required. As in the case of the planar rectilinear grid, this is a practical consideration that, while perhaps almost arbitrary from a mathematical viewpoint, cannot be ignored in the short term.

14. The grid system contains grids of any arbitrarily defined spatial resolution.

We have already noted that it is mathematically impossible for any global point grid or surface tessellation to completely fulfill all of these criteria, as several are mutually exclusive. A good general-purpose grid or tessellation might be expected to strike a balance among all the criteria, whereas those tuned for specific applications or numerical methods might value certain of these criteria more highly. For example, geostatistical methods favor equal-area tessellations that completely cover the globe and have a hierarchical structure. Survey sampling designs for global environmental monitoring have equal-area cells as a prime requirement, whereas atmospheric transport modeling equations rely on criterion seven. Scientists involved in GIS data integration and cartographic display, on the other hand, may value highly the last three criteria.

Evaluation Criteria Metrics

Global grid evaluation criteria are of limited utility unless metrics suitable for grid comparison are developed for each. Both topological and geometrical metrics must be devised for 1) checking that a criterion has been met, and 2) determining how well a criterion has been satisfied. Examples of the first type of metrics include:

- Criterion 1—Ensure that the sum of cell areas equals the sea level surface area of the globe, and that the coordinates of all shared cell edges are identical.
- Criterion 6—Check that the coordinates defining each cell edge are identical to those computed from the linear equation determined for the edge endpoints.
- Criterion 9—Employ a point-in-polygon function to check that only one sampling point lies in each cell.
- Criterion 8—Check to see that recursive partitioning, a mathematical procedure essential to create a hierarchical grid system can be performed.

The terminology of recursive partitioning is best understood from an illustration such as Figure 2. Two types of partitioning, called 4-fold and 9-fold, are shown in the top and bottom triangular cells. This involves checking that each full triangle (recursion level 0) can be partitioned into either 4 or 9 triangular cells (recursion level 1). If this 4- or 9-fold partitioning can be continued to produce subtriangles at all higher levels of recursion, a hierarchical triangular grid system is achievable.

Recursive partitioning facilitates the inverse operation of subcell aggregation into larger cells of the same or a different geometrical form. For example, the left half of Figure 2 illustrates that sets of 4, 9, 16, 25,... neighboring subtriangles can be assembled into progressively coarser spatial resolution triangular global grids. The right half of this figure shows that sets of 6, 24, 96,... neighboring subtriangles can be assembled into progressively larger hexagonal cells. Notice that with 9-fold partitioning the hexagonal cells are oriented identically, an advantage when assembling global data sets at varying spatial resolutions. A similar illustration could be created for recursive partitioning of spherically rectangular quadrilaterals, with the desirable rotational invariance present for any n-fold partitioning.

We have focused on geometrical comparison of metrics for surface area, compactness, and point spacing on both the sphere and a spheroid such as the GRS80 or WGS84. We were aware that measures on the sphere and spheroid would give nearly identical numerical results, but using spheroidal area metrics was essential to our demonstration that certain grids are truly equal area on the Earth's surface. All of these measures involve determination of geodesic distances using standard ellipsoidal distance equations (Bomford 1971). Examples of comparison metrics include:

- Criterion 2—The spheroidal surface area of quadrilateral cells can be computed using standard equations found in Maling (1992). Computing the spheroidal surface area of

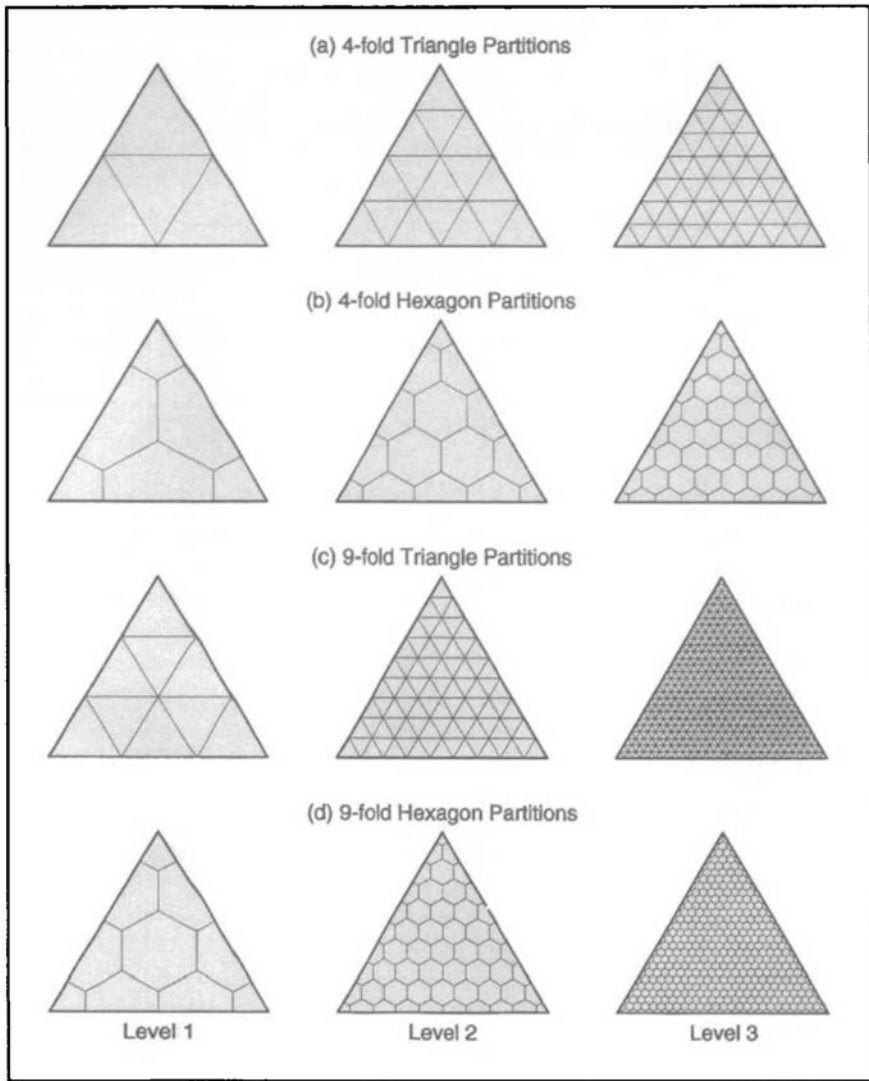


Figure 2. Four- and 9-fold triangular and hexagonal partitioning of an icosahedron face at the first three levels of recursion.

cells with great circle edges (such as spheroidal triangles or hexagons) or of more geometrically complex cells requires the oriented triangle summation approach found in Kimerling (1984). These actual areas were normalized through dividing by the average area for all cells in the tessellation, so that all cells in a perfectly equal area global grid would have normalized cell areas of 1.0.

- Criterion 5—Planar compactness is often measured by the surface-area-to-perimeter ratio (Muehrcke and Muehrcke 1997). Standardizing this ratio to 1.0 for a planar circle of the same area as the cell gives a compactness index applicable to all discrete global grids. This index is computed from the equation:

$$2 \times \text{sqrt}(\pi \times \text{cell area}) / \text{cell perimeter} = \\ = 3.545 \times \text{sqrt}(\text{cell area}^2 / r^2) / \text{cell perimeter} \quad (1)$$

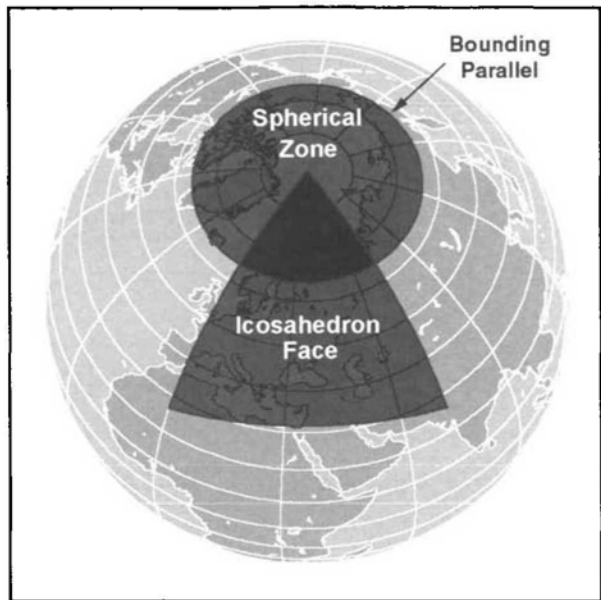


Figure 3. Spherical zone used in Zone Standardized Compactness (ZSC) calculation for an icosahedron face.

However, we are dealing with cells on the globe. Taking the Earth's sphericity into account, a better index is one that uses a pole-centered spherical zone of the same area as the grid cell (Figure 3) for the ideal (1.0) compactness. What we term Zone Standardized Compactness (ZSC) is computed from:

$$ZSC = \sqrt{4\pi \times \text{cell area} - \text{cell area}^2/r^2}/\text{cell perimeter} \quad (2)$$

The derivation of ZSC is given in the Appendix. We have extended this idea to the spheroid by determining the spheroidal area to parallel perimeter ratio, normalized to a spheroidal cap of the same surface area as the cell (Kimerling et al. 1995).

- Criterion 11—Grid point spacing can be measured, assuming that we can determine the latitude and longitude of points within adjacent cells. Assuming the globe to be spherical, we employ the standard great circle distance equation for each pair of adjacent coordinates:

$$\text{distance} = r * \arccos(\sin(lat_1) * \sin(lat_2) + \cos(lat_1) * \cos(lat_2) * \cos(|lon_1 - lon_2|)) \quad (3)$$

- Criterion 10—Determining grid point centrality within a cell can be approached as a center of gravity problem. Here we can use off-the-shelf algorithms for center-of-gravity computation from lists of edge coordinates, and then compare the grid point location to the center of gravity to determine the distance and direction of deviation.

Each of the above comparison metrics are computed for a single cell or grid point and can be analyzed statistically when computations are extended to the entire globe (realizing that the entire population of cells is the sample). The mean standard deviation and the range of cell metrics have been found to be useful comparison statistics for alternative global grids (White et al. 1998).

Global Grid Alternatives

Numerous surface tessellations have been proposed as global grids, but the possibilities can be organized into a limited number of general categories. Inspired by Dutton's (1994) general tessellation taxonomy, we developed a more specific hierarchical classification scheme for global grids (Figure 4), and then selected grids from different classes for comparison. At the broadest level, our scheme divides grids into those based on directly tessellating the sphere or spheroid, and those that transform all or a portion of the globe to a map projection surface which is tessellated in a regular manner, with cell edges and/or grid points then back-projected to the sphere or spheroid.

At the second level in our classification hierarchy, direct surface tessellations can be based on:

- Subdividing quadrilateral cells recursively;
- Subdividing the faces of a spherical Platonic polyhedron recursively, or
- Creating a Voronoi tessellation comprised of spherical or spheroidal Thiessen polygons.

Directly tessellated quadrilateral grids can be further divided into what the global modeling community calls equal-angle and “constant-area” grids (Kahn 1995). Tessellations of the globe into quadrilateral cells of equal latitudinal and longitudinal extent are termed equal angle. Examples abound, including the 5' x 5' ETOPO5 global DEM, and the ERBE 2.5° x 2.5°, 5° x 5°, and 10° x 10° grids (Brooks 1981). Constant-area tessellations begin with an arbitrarily sized quadrilateral cell at the equator, and then define the parallel and meridian cell boundaries across the globe so as to achieve approximately equal-area cells. This is done either by keeping the latitude increment constant and adjusting the longitude increment as the pole is approached, or vice versa (Brooks 1981).

Directly tessellated polyhedral grids can also be divided into two categories, based on whether the partitioning of polyhedral faces is performed with the edges of a great or a small circle. Fekete and Treinish's (1990) spherical quadtree data structure, which is based on recursive subdivision of spherical triangles obtained by projecting the faces of an icosahedron onto a sphere, is a good

example of great-circle edge partitioning. Song's (1997) small-circle subdivision system creates equal-area spherical triangles with more mathematically complex small circle edges. Dutton's (1988) QTM projection grid for octahedron faces is an interesting combination of great- and small-circle subdivision.

Lukatela's (1987) Hipparchus Geopositioning Model is an excellent example of a spheroidal Voronoi tessellation. Here the outwardly simple problem is computing a set of regularly spaced grid points from which spherical or spheroidal Thiessen polygons can be constructed. But as Giacaglia and Lundquist (1972) note: "The problem of distributing in the most regular way a given number of points on a sphere has been studied for centuries and, in general, is still unsolved." Methods such as finding the greatest number of small circles of a given radius that can be placed on a spherical surface without overlapping (Coxeter 1962) have been superseded by sampling function approaches for the sphere that begin with the edges of a spherical polyhedron (Giacaglia and Lundquist 1972). Perfect regularity, however, remains an inherently unachievable ideal.

Map projection based global tessellations currently can be placed in one of two categories: single and multiple projection surfaces. Single projections of the globe, typically cylindrical, have been used to construct quadrilateral grids. It is useful, due to the importance of satisfying criterion two, to further divide projection surfaces into equal area (e.g., Tobler and Chen's (1986) Lambert cylindrical equal-area grid) and non-equal area (the ETOPO 5 grid, for example, can be thought of as a square projection partitioned into cells 5' x 5' in length on the projection surface) categories. Multiple projection surfaces are typically faces of Platonic polyhedra. We can also place these into equal area (e.g., Snyder (1992) polyhedral equal area projections for the five Platonic polyhedra) and non-equal area (e.g., Fuller (1982) and Baumgardner and Frederickson (1985)) projection of icosahedron faces.

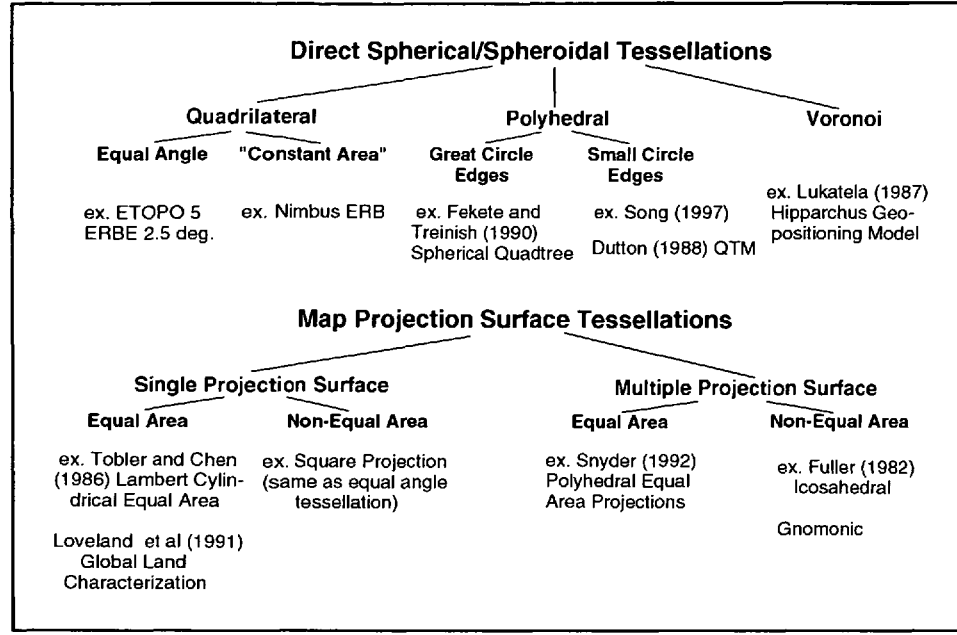


Figure 4. Global grid taxonomy.

Global Grid Comparison Examples

Our overall comparison of the above categories of global grids, based on the Goodchild criteria, is presented in Table 1 and will be discussed as part of our recommendations. We have also selected four examples from different categories in our taxonomy to illustrate our more detailed comparison of surface area, compactness, and centerpoint spacing variation. These examples, described below, were selected to show the fundamental geometrical differences between quadrilateral and polyhedral grids, as well as to contrast commonly used "standard" quadrilateral grids with polyhedral alternatives.

Equal-Angle Quadrilateral Tessellation

Our example will be an initial partitioning of the globe into thirty-two $45^\circ \times 45^\circ$ cells at recursion level 0, and subsequent 9-fold recursive partitioning to level five. Hence, grids with $45^\circ \times 45^\circ$, $15^\circ \times 15^\circ$, $5^\circ \times 5^\circ$, $1/2/3^\circ \times 1/2/3^\circ$, $5/9^\circ \times 5/9^\circ$, and $5/27^\circ \times 5/27^\circ$ edges will be analyzed. Recursion level two, illustrated in Figure 5, corresponds to the $5^\circ \times 5^\circ$ ERBE grid.

Constant-Area Quadrilateral Tessellation

Our example is the Nimbus Earth Radiation Budget (ERB) Experiment grid with initial $4.5^\circ \times 4.5^\circ$ quadrilateral cells at the equator (Figure 6). The longitudinal increment increases in 12 discrete steps to 120° near each pole. Recursive partitioning into approximately constant-area subcells is more problematic, as 2-frequency equal-angle partitioning is commonly

Equal Angle Grid

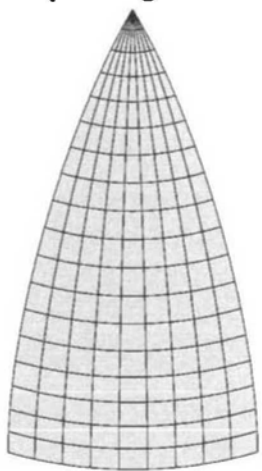


Figure 5. Equal-angle quadrilateral grid for a 45° longitude by 90° latitude section of the globe.

"Constant" Area Grid

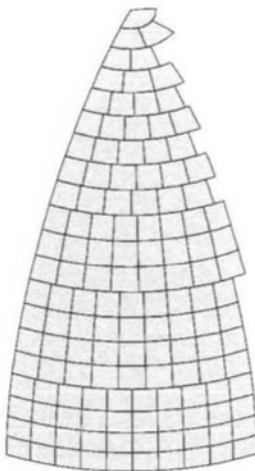


Figure 6. Constant area quadrilateral grid for a 45° longitude by 90° latitude section of the globe.

employed for simplicity. Breaking from tradition, we employ 3-frequency equal-angle partitioning to maintain consistency in our comparisons while using the same basic partitioning method. The initial 4.5° latitude x variable longitude cells correspond approximately to recursion level two in our equal-angle tessellation, with partitioning carried to recursion level 5 (1.5°, 0.5°, 1.6° latitude by variable longitude cell edges).

Equal-Area Map Projection Surface Tessellation

Our example is the Icosahedral Snyder Equal-Area (ISEA) projection (Snyder 1992) which transforms each icosahedron face on the globe into an equilateral planar triangle while maintaining area

equivalence throughout (Figure 7). The projection is made equal area by adjusting the scale outward from the center of each edge. This results in increased shape distortion as each of the three axes from the triangle center to corner vertices is approached. A map of angular deformation across an icosahedron face (which is the result of our Tissot distortion analysis based on the Gaussian basic quantity approach outlined in Maling (1992)) shows this pattern of distortion.

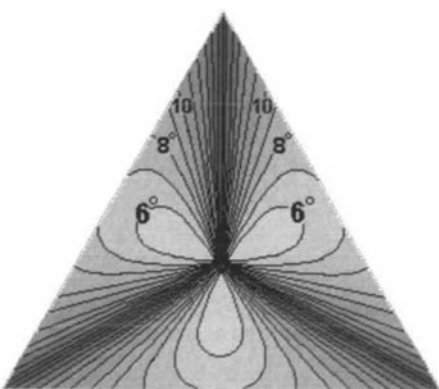
The equilateral triangular projection of each icosahedron face is subdivided recursively into equilateral subtriangles in either the 4-fold or the 9-fold manner illustrated in Figure 2. The bowing of triangle edges along the three axes of angular deformation is apparent in Figure 8 where 4-fold subdivision subtriangles of recursion level four are back projected to the globe. This edge bowing is a primary cause of variations in compactness among subtriangles.

We noted earlier that triangular grids allow hexagonal grids to be created through subtriangle aggregation, and that hexagonal grids have several advantages related to global data analysis. The ISEA triangular grid inherently allows equal-area hexagons to be assembled at varying

SNYDER MAP PROJECTION



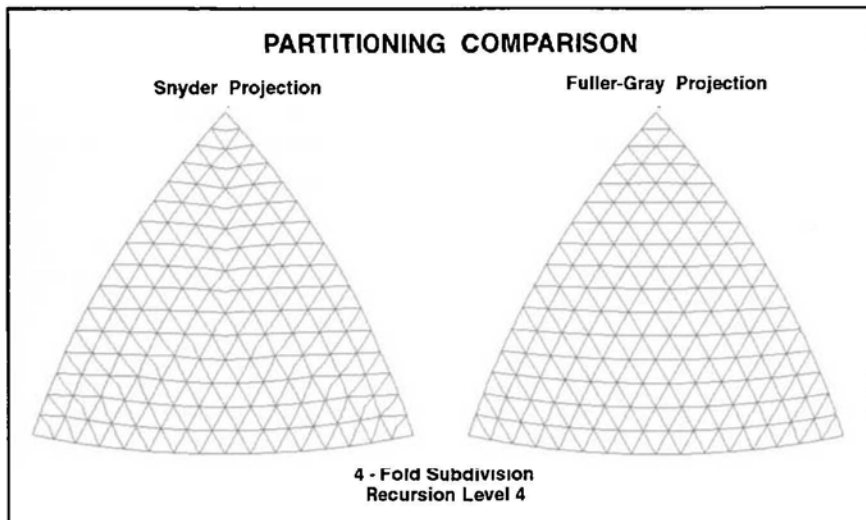
Icosahedron Face



Tissot Angular Deformation

Figure 7. Icosahedral Snyder Equal Area (ISEA) projection of an icosahedron face (a); Tissot angular deformation isolines (b).

Figure 8. Icosahedron faces that are 4-fold partitioned to recursion level four on the ISEA and Fuller-Gray projection surfaces, then re-projected on an orthographic map projection to simulate the Earth's sphericity.



levels of spatial resolution. For example, aggregating sets of 54 neighboring triangles produces the equal-area hexagonal grid for the icosahedron face shown in Figure 9a. Again apparent is the bowing of hexagon edges along the three axes of higher angular deformation, which should introduce larger compactness variations.

Aggregating the same subtriangles into sets of six neighbors (Figure 9b) creates a nine times higher resolution hexagonal grid with edge bowing more localized along the three axes. Because nine of the small hexagons (seven full and one-third of six adjacent) form the large hexagon, the small hexagons are a 9-fold subdivision of the large hexagons at the next higher level of recursion. Further 9-fold partitioning of the underlying subtriangles allows assembly into 9-fold smaller hexagons at higher levels of recursion.

Non-Equal Area Map Projection Surface Tessellation

We will use the Fuller-Gray projection which is based on the geometrical idea behind R. Buckminster Fuller's icosahedral world map projection (Fuller 1982). Fuller imagined the three edges of each icosahedron face as flexible bands curved to lie on the spherical surface (left half of Figure 10). Each edge would be subdivided and holes drilled at n equally spaced increments, and flexible bands would be strung between corresponding holes on adjacent edges. This would create a triangular network of lines on the sphere, which could be flattened to create a regular grid of equilateral subtriangles (right half of Figure 10).

Fuller imagined the vertices of each subtriangle being the projection of the corresponding line intersection point on the sphere. These intersection points were later found physically impossible to achieve, because each triplet of intersecting lines on the globe forms a small triangle in the plane, whose centerpoint is the best approximation of Fuller's idea. Gray (1994) developed exact transformation equations for this approximation, producing a compromise projection having both small area and shape distortion.

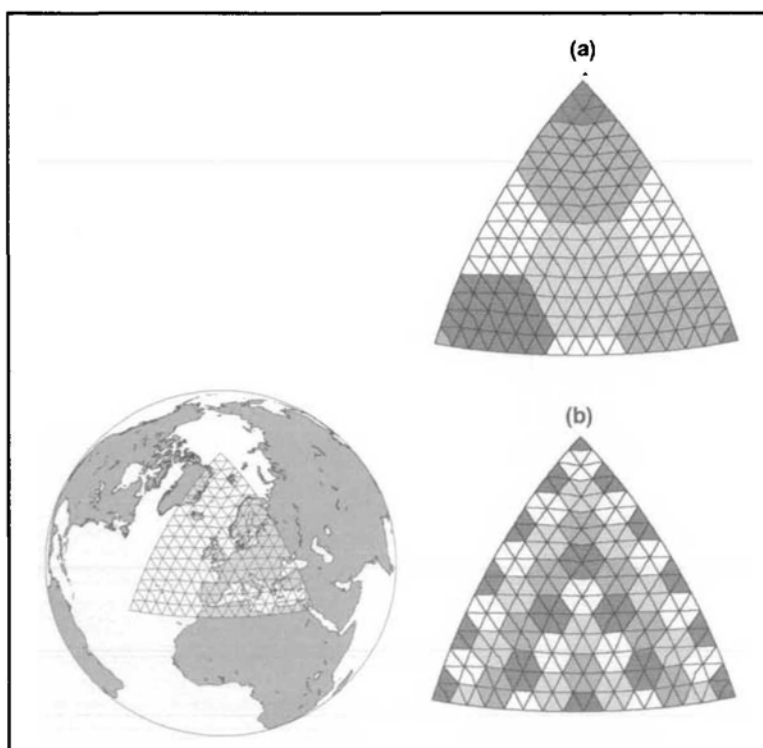


Figure 9. Aggregation of 54 and 6 neighboring triangles on the ISEA projection into equal area hexagonal cells forming 9-fold higher resolution grids.

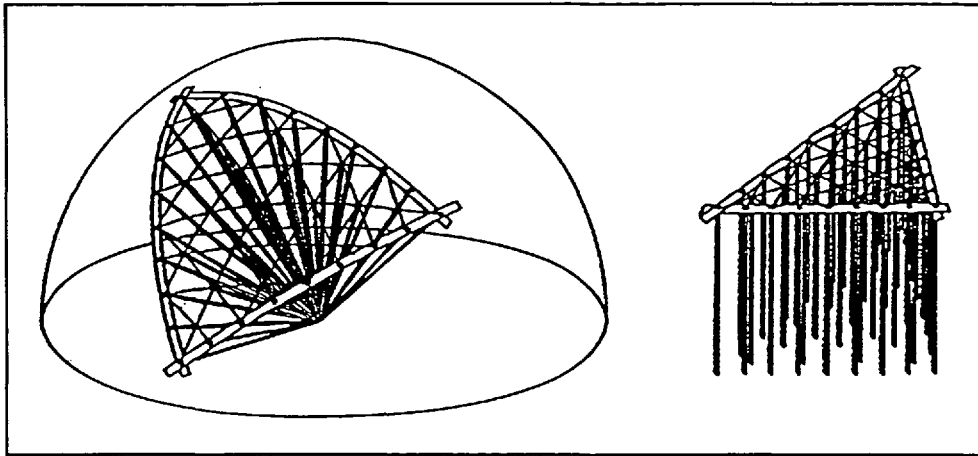


Figure 10. Fuller's geometrical concept of an icosahedral map projection surface (Source: Fuller 1982).

The equilateral-triangle Fuller-Gray projection of an icosahedron face is shown in Figure 11, along with area-scale and angular-deformation maps displaying results of our Tissot distortion analysis. Note the smooth increase in area-scale and angular deformation from the triangle center to each edge vertex. Both recursive partitioning and triangle aggregation is performed identically to the Snyder projection. The only difference should be the creation of non-equal area triangular and hexagonal cells that vary less in compactness on average and that grade smoothly from slightly higher to lower compactness (Figure 8).

Analyses and Results

The ideal comparison of global grid geometrical properties would consist of computing surface area, compactness, and other metrics at each level of recursion down to the spatial resolution corresponding to the smallest grid cell expected to be used in global analysis. If the smallest cell were 1 km^2 , for example, the 9-fold partitioning of an icosahedron face must be carried out to recursion level eight, meaning that area, compactness, centerpoint distance, and other metrics must be computed for over 500 million cells. Naturally, an infinite number of triangular, hexagonal, or quadrilateral recursion levels and cells are possible, as recursive partitioning can continue indefinitely.

We have found 9-fold partitioning to recursion levels less than six to be suitable for comparison purposes, because surface area, compactness, centerpoint spacing, and other metrics are still computable at the rapidly increasing cell densities. However, the computation effort quickly becomes immense at higher levels of recursion and the results may not add significantly to our understanding of the surface

tessellation or grid point geometry.

The normalized area, zone standardized compactness and centerpoint distance analyses that follow are a representative sample of our full research effort. The four grid alternatives examined were selected from the 10 we studied, but results from only two of the five recursion levels we examined are presented here to illus-

trate the essential geometrical properties of the full range of quadrilateral and polyhedral grid alternatives. We have limited the polyhedral analysis to the hexagonal tessellation, because area and shape distortion characteristics of triangular partitioning are presented in a companion article (White et al. 1998).

Normalized Area Map Comparison

- Spheroidal areas were computed from sets of closely spaced geodetic latitude and longitude coordinates along each cell edge (usually 11 points along an edge). For the two quadrilateral tessellations the bounding parallels were on the WGS 84 spheroid. However, for the Fuller-Gray and Snyder projections only spherical equations were available, so a more complex spheroidal transformation procedure had to be used. This involved Projecting from the authalic sphere for the WGS 84 ellipsoid to the plane using forward projection equations;
- Partitioning on the planar projection surface;
- Back projecting cell edges and centerpoints to spherical coordinates using the inverse spherical equations for each projection; and
- Converting authalic to WGS 84 geodetic latitude using the transformation equations found in Snyder (1987). This allows the oriented spheroidal triangle summation method (Kimerling 1984) to be applied to the four (and other) global grid alternatives.

Maps comparing variations in normalized surface area for the four discrete global grid examples described above are presented in Figure 12. The equal-angle and constant-area grids cover 45° of longitude by 90° of latitude (equator to

Fuller-Grey map projection

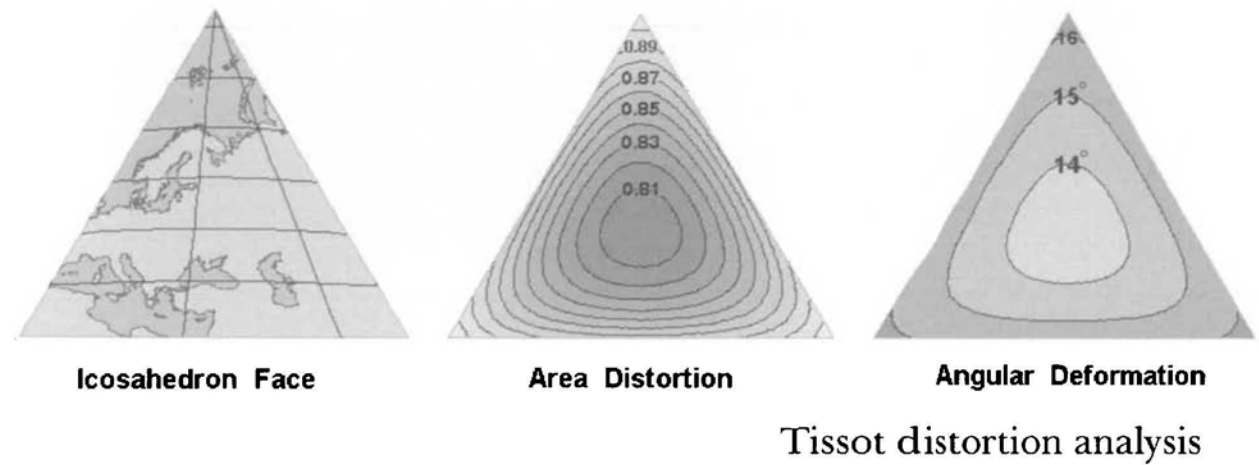


Figure 11. Fuller-Grey map projection and Tissot distortion analysis for an icosahedron face.

pole), or 1/16th of the globe. Each icosahedron face, of course, covers 1/20th of the globe, so that the surface areas of comparison surfaces are approximately the same. The level of recursion for each grid was selected so that the average cell area within each grid is nearly the same. From these maps in Figure 12, it is apparent that:

- The larger range in normalized area (0.069 - 1.569 or 150 percent) associated with the equal-angle grid makes it, as expected, by far the worst alternative of the four;
- The constant-area grid has a greater range of normalized area than either the Snyder or Fuller-Grey grids. The pattern of spatial variation is one of identical normalized area within east-west bands. Cell areas also decrease slowly from south to north within the three blocks in the bottom half of the map having identical meridians as cell boundaries. Such regularity is not present in the rows of cells forming the top half of the map;
- Normalized hexagon areas on the Fuller-Grey projection decrease smoothly from a value of 1.06 (6 percent above average) at the icosahedron face center to a lower value of 0.944 near each corner. The very low normalized area for the triangle at each corner is caused by this being one of five spherical triangles on adjacent icosahedron faces that together form one of 12 pentagonal cells on the globe. Each pentagon area is 5/6th that of the average hexagonal cell, which gives the lower normalized area;

- Normalized hexagon areas on the Snyder projection are identical and just slightly larger than 1.0 so as to offset the three smaller areas of corner pentagonal cells. If the pentagon areas are removed from the calculations, all hexagons are measured as having a 1.0 normalized surface area, a numerical demonstration that the Snyder equations for the icosahedron do indeed produce an equal area map projection surface.

We next examine the spatial pattern of normalized area for hexagons at recursion levels three and four for the 9-fold partitioning of the Fuller-Grey and Snyder projection surfaces. The results are presented in the four orthographic map projections of icosahedron faces shown in Figure 13. In each of the three Snyder projection grids, the normalized areas of hexagonal cells are identical, but the normalized area value of the grid rapidly approaches 1.0 as the level of recursion increases. This is due to the progressively smaller contribution of the pentagonal corner cells to the total area of the icosahedron face.

At increasing levels of recursion, the Fuller-Grey projection grids show a progressive smoothing of normalized area variation as the level of recursion increases. By the fourth level the smooth pattern of reduction in normalized area from the icosahedron center toward each edge closely mirrors the Tissot area distortion isolines defining the continuous area distortion surface. As expected, the spatial pattern of continuous Tissot area distortion and of discrete normalized cell

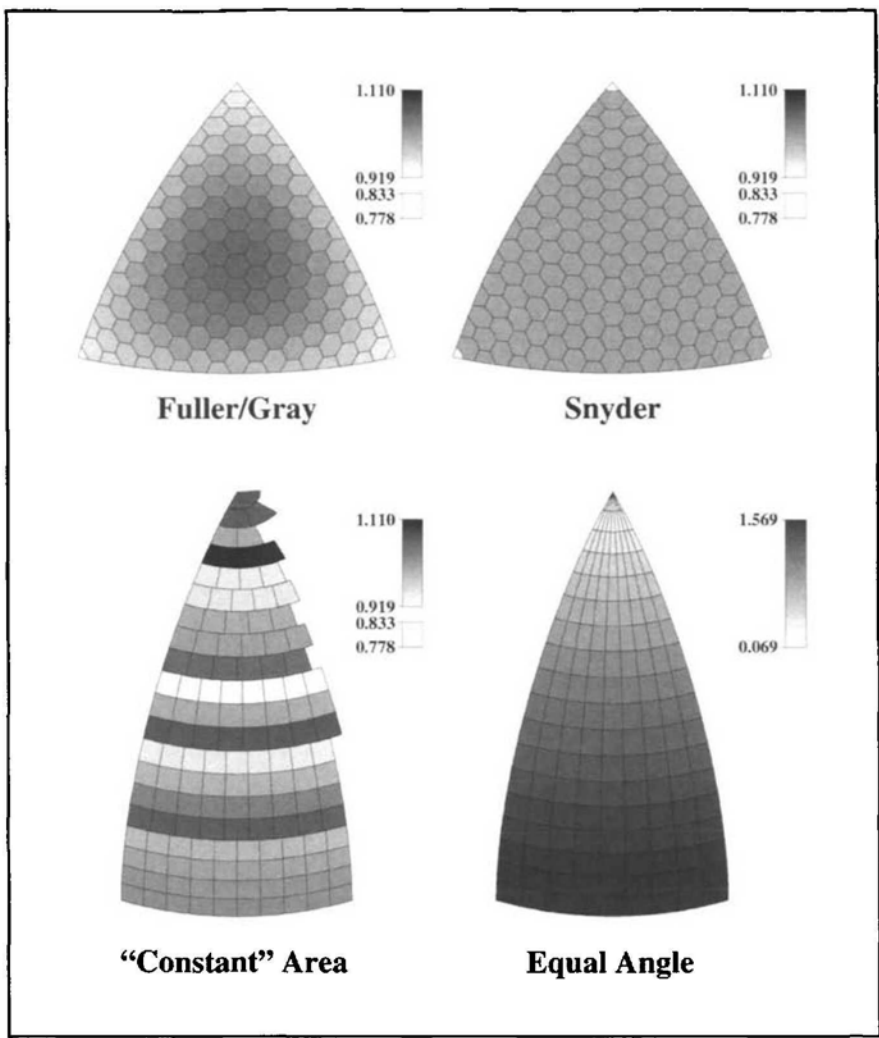


Figure 12. Normalized-area comparison for basic segments of four global grids, each shown on an orthographic map projection to simulate the Earth's sphericity.

areas become indistinguishable at higher levels of recursion.

Compactness Map Comparison

Results from computation of Zone Standardized Compactness (ZSC) for the four grid alternatives are presented in Figure 14. The portions of the globe covered and levels of recursion selected for the area comparisons are used here as well to insure that the average cell area of each grid is similar. These four ZSC maps show that:

- Compactness variation is greatest by far for the equal-angle grid, as the basic cell shapes vary from narrow spherical triangles at the pole to spherical squares at the equator;
- There is relatively little variation in compactness across the constant-area grid, in spite of the cell at the pole being triangular in shape

and the other cells becoming progressively more square in shape as the equator is approached;

- The Snyder grid center hexagon has the lowest compactness (ignoring the inherently lower compactness pentagon segments at each corner). The bowed pairs of hexagon edges along each axis of higher angular deformation produce lower compactness hexagons than those farther away from each axis, where higher ZSC values vary only slightly; and
- Except for the lower compactness corner pentagon cells, ZSC values across the Fuller-Gray grid are consistently higher than the other three alternatives, with the highest value at the icosahedron center and a slight, smooth decrease radially outward from the center.

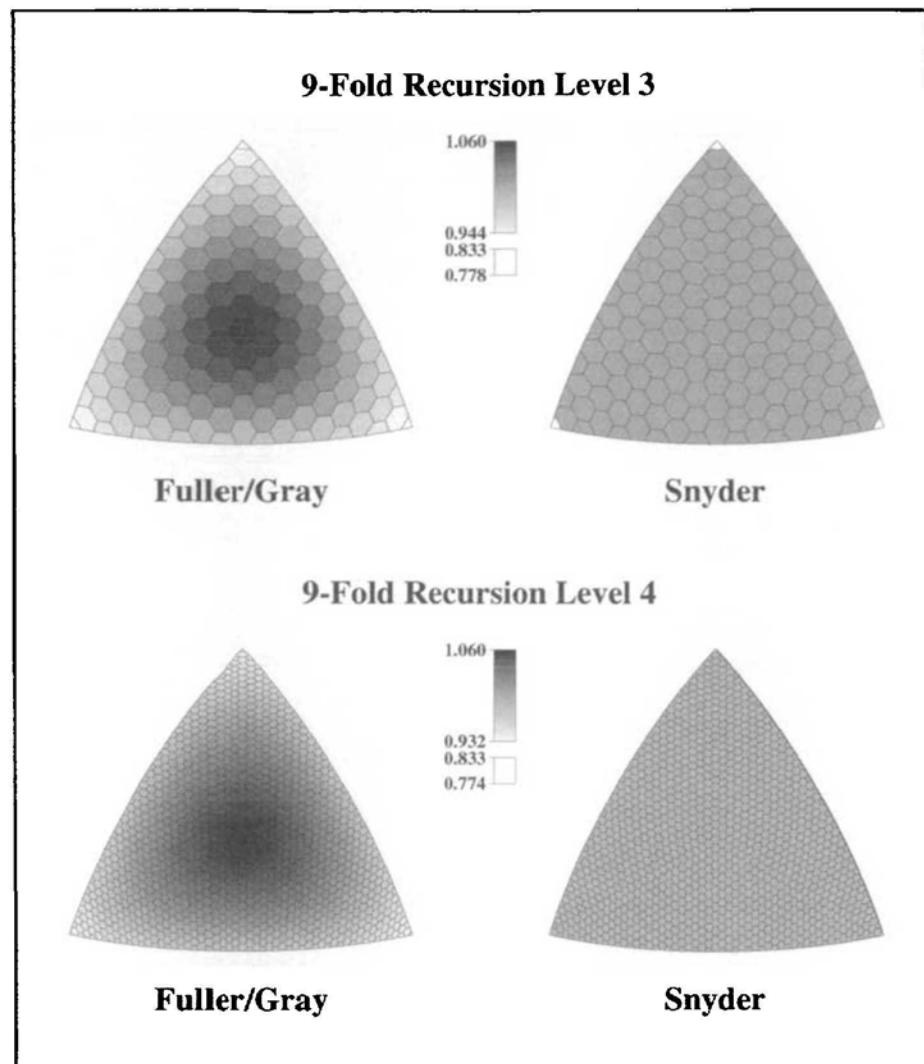
As done with normalized area, the spatial pattern of ZSC for hexagonal grids 9-fold partitioned to recursion levels three and four was examined for the Fuller-Gray

and Snyder map projection surfaces (Figure 15). Both grids show a progressive smoothing of ZSC values, also seen in the area analysis, with increasing levels of recursion. In both grids the spatial pattern of slightly lower to higher compactness closely mirrors the Tissot angular deformation isoline pattern for the map projection, becoming spatially indistinguishable by recursion level four. Hence, Tissot angular deformation can be used to predict the spatial pattern of compactness variation.

Centerpoint Distance Map Comparison

Figure 16 displays maps of an icosahedron face on the Fuller-Gray and Snyder projection surfaces that depict variations in centerpoint distance between adjacent hexagons for 9-fold hexagonal partitioning at three levels of recursion (similar research on

Figure 13. Normalized-area comparison for two recursion levels of the Fuller-Gray and ISEA grids, each shown on an orthographic map projection to simulate the Earth's sphericity.



quadrilateral centerpoint distance for the equal-angle and constant-area grids is underway). This example of our centerpoint distance analysis shows how variations in great-circle distance between adjacent pairs of hexagon centers can be mapped.

The six equilateral triangles forming each hexagon can be thought of as map symbols shaded according to the distance between the hexagon center and the centerpoint of adjacent hexagons to the north (0°), northeast (60°), southeast (120°), south (180°), southwest (240°), and northwest (300°), assuming north to be at the top of the page.

At the lowest level of recursion (top-right map), the general pattern of larger (darker gray) and smaller (lighter gray) distances relative to the average (medium gray) centerpoint to centerpoint distance are aligned with the three axes of higher angular deformation for the Snyder projection, as we would expect. The shortest distances are along each axis and the longest distances are adjacent and roughly perpendicular to each axis. This spatial pattern of centerpoint distance variation

persists and becomes better defined at the next two higher levels of recursion. At the highest level examined here (bottom-right map), the larger and smaller distances clearly are localized along each axis, grading toward average values in a “propeller-like” pattern that corresponds with the Tissot angular deformation isolines. Indeed, the Tissot diagram in Figure 7 is an excellent predictor of where variations in centerpoint distance should occur on the Snyder grid.

The spatial pattern of centerpoint distance variation for the hexagonally partitioned Fuller-Gray projection surface is not easily discerned at the lowest level of recursion (upper-left map), but becomes readily visible at the next two higher levels. As with the Snyder projection, Tissot angular deformation isolines predict the spatial pattern of little variation in the center of the icosahedron face, with progressively larger centerpoint distance variations (often in longer-shorter distance adjacent pairs) as each edge is approached. Overall there appears to be slightly less centerpoint distance variation on the Fuller-Gray

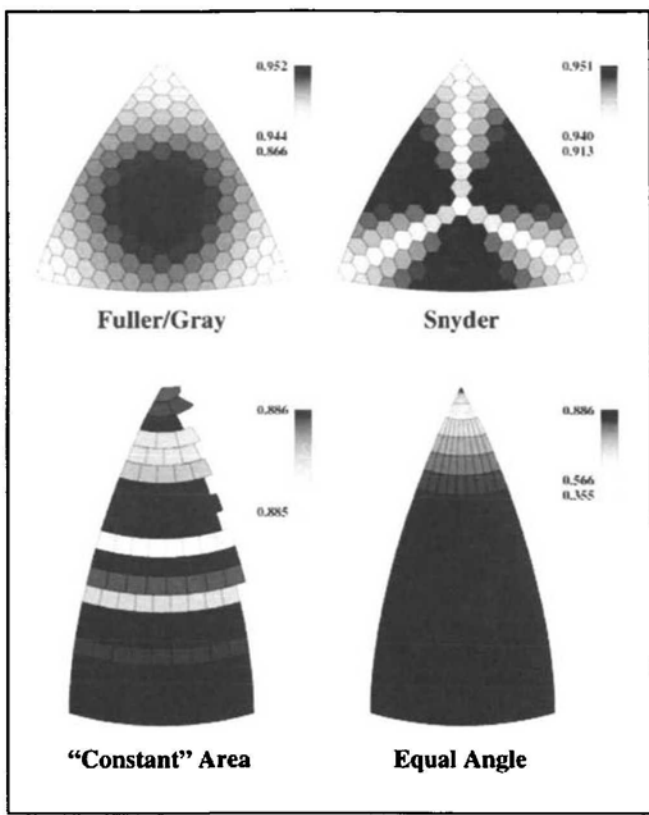


Figure 14. Compactness comparison for basic segments of four global grids, each shown on an orthographic map projection to simulate the Earth's sphericity.

hexagonal grid, but this can only be shown conclusively by a statistical comparison of alternative grids.

Statistical Comparison Results

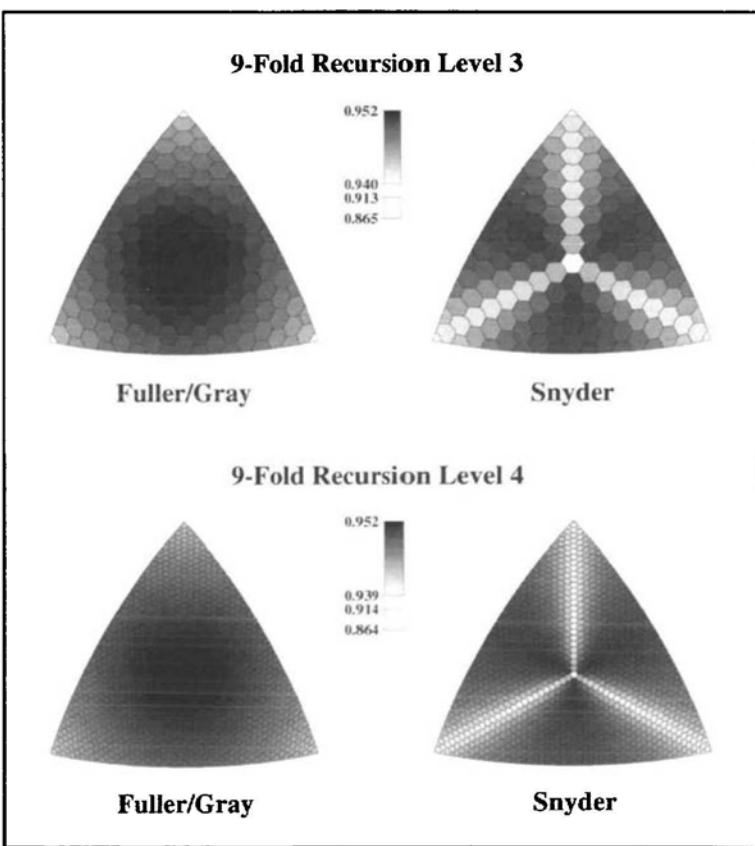
Because variation in cell surface area is a major concern for geostatisticians and others, we analyzed the variation in normalized cell area with increasing levels of recursion. Figure 17 is a logarithmic graph of the standard deviation in normalized-cell area versus the decreasing average-cell area at increasing levels of recursion for the four discrete global grid alternatives (but only the hexagonal grids formed by Snyder and Fuller-Gray projection subtriangles) examined graphically above. Recognizing that the hexagonal partitioning of

Figure 15. Compactness comparison for two recursion levels of the Fuller-Gray and ISEA grids, each shown on an orthographic map projection to simulate the Earth's sphericity.

the icosahedron face always creates 12 pentagons on the globe exactly 5/6th the area of each hexagon, the surface area standard deviation for the Snyder grid will always be slightly greater than zero, even though there is no area variation among the hexagons formed. However, at progressively higher levels of recursion, the 12 pentagons occupy increasingly less of the total surface area and the standard deviation for the entire globe rapidly approaches zero. Hence, this graph shows the Snyder grid to be clearly superior for hexagonal subcells less than 100,000 km² in area.

Variation in centerpoint spacing between adjacent cells for the four grid alternatives can be analyzed by graphing logarithmically the standard deviation in normalized centerpoint spacing against average cell area at increasing levels of recursion (Figure 18). This graph shows the grids to perform similarly, except for the poorly performing Equal Angle Quadrilateral grid. The Fuller and Constant Area Quadrilateral grids converge at higher recursion levels to essentially identical low standard deviations, closely followed by the Snyder grid.

Average subcell compactness values for the four grids (Figure 19) shows the superior performance of icosahedral models over quadrilateral, which is to be expected since hexagonal shapes are



inherently more compact than rectangular shapes. At all levels of recursion the Fuller grid is comprised of hexagons slightly more compact than corresponding Snyder grid hexagons, both being far more compact than the corresponding constant area and equal angle grid quadrilaterals.

Variation in subcell compactness, seen by graphing the standard deviation of cell compactness values against average cell area (Figure 20), shows the slightly better performance of the Fuller grid over the Snyder grid at higher levels of recursion. The constant-area grid has the lowest overall standard deviation at its initial resolution (level 0), but its standard deviation increases rapidly as the initial cells are partitioned in an equal-angle manner. However, the poor performance associated with the equal-angle grid at all levels of recursion is never approached.

Summary Rankings

In addition to the detailed numerical analysis of grid-cell area, compactness, and center-point spacing at different levels of recursion, we carried out an overall comparison of numerous

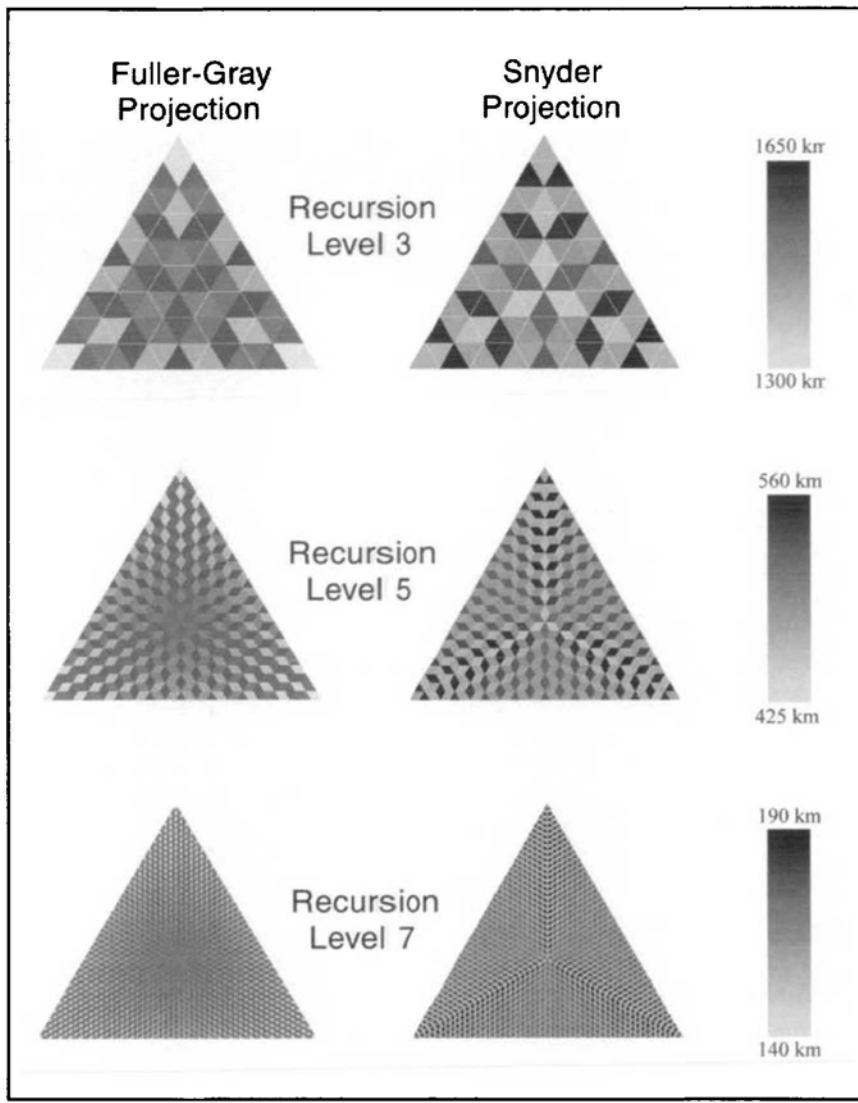
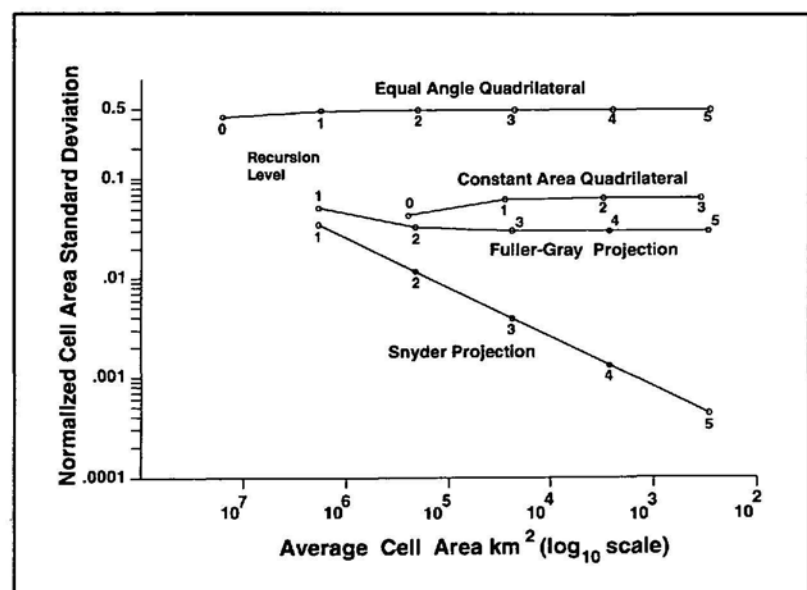


Figure 16. Variations in hexagonal centerpoint spacing at three levels of recursion for the Fuller and ISEA Grids on an icosahedron face.



discrete global grid alternatives, including the seven presented in Table 1. Eleven of the fourteen Goodchild criteria were investigated, along with two related criteria deemed significant for global grid comparison. For Goodchild criteria 2, 4, and 5, a summary ordinal ranking from 1 (very poor) to 10 (best possible) was developed based on the quantitative analysis of comparison metrics.

Table 1 provides information crucial to the selection of a global

Figure 17. Normalized subcell area standard deviation vs. average cell area for four global grids.

Criterion	Equal Angle	Constant Area	Snyder	Fuller-Gray	Small Circle	Dir. Sphere	Gnomonic
1. Domain is globe	yes	yes	yes	yes	yes	yes	yes
2. Equal area ¹	1	7	10	8	10	6	3
3. Same topology	yes	no	yes	yes	yes	yes	yes
4. Equal shape ¹	1	3	7	8	7	9	9
5. Compactness ¹	1	4	7	8	8	8	9
6. Straight edges on projection	n.a. ²	n.a.	yes	yes	n.a.	n.a.	yes
7. Perimeter bisection	n.i. ³	n.i.	n.i.	n.i.	n.i.	n.i.	n.i.
8. Hierarchy	yes	yes	yes ⁴	yes ⁴	yes ⁴	yes ⁴	yes ⁴
9. Single point	yes	yes	yes	yes	yes	yes	yes
10. Maximally centered	n.i.	n.i.	n.i.	n.i.	n.i.	n.i.	n.i.
11. Equidistant	no	no	no	no	no	no	no
12. Addressing	n.i.	n.i.	n.i.	n.i.	n.i.	n.i.	n.i.
13. Latitude/Longitude	yes	yes	yes	yes	yes	yes	yes
14. Arbitrary resolution	yes	yes	yes	yes	yes	yes	yes
Geodesic edge lines	no	no	no	no	no	yes	yes
Spatial nature of area variation	Continuously varying	Part continuous, part irregular	Constant	Continuously varying	Constant	Fractal-like	Continuously varying

¹Best possible = 10; very good = 9; → very poor = 1.

²n.a. = not applicable.

³n.i. = not investigated.

⁴Only the triangular cells, not the hexagonal, are hierarchical in these grids.

Table 1. Evaluation of Goodchild's and related comparison criteria for different global grids.

grid based on the relative importance of evaluation criteria from the user's perspective. If cell compactness is of prime importance, for example, a triangular or hexagonal grid based on partitioning a Gnomonic map projection of an icosahedron face (not discussed in this article) would be the best alternative, closely followed by direct

spherical subdivision, the small circle subdivision method, and the Fuller-Gray map projection for the icosahedron. If good overall performance is of paramount concern, the triangular and/or hexagonal partitioning of the Fuller-Gray projection surface might be selected due to the low variation in compactness of highly compact cells that vary slightly in area in a continuously varying, predictable manner.

Conclusions

The global grid evaluation criteria and associated metrics have allowed us to compare grids varying widely in cell geometry and topology. We have observed that the prime areas of concern among the small portion of the global data user community we have interacted with to date are equal-area cells and a nested

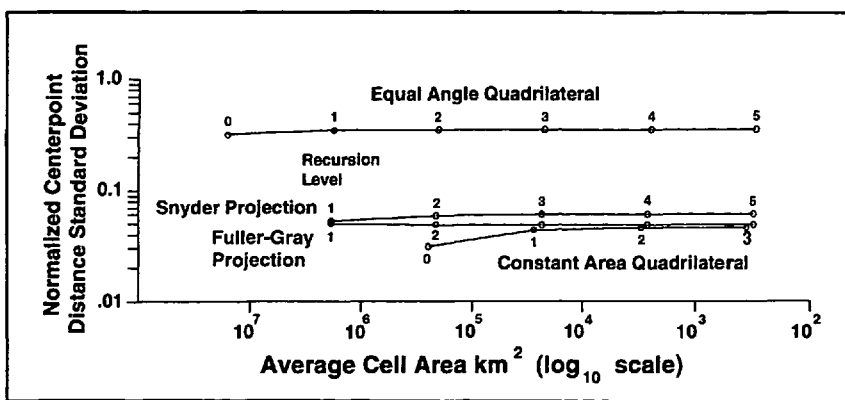


Figure 18. Normalized centerpoint distance standard deviation vs. average cell area for four global grids.

hierarchy among cells (criteria 2 and 8). Both the quadrilateral grids and triangular forms of polyhedral grids examined here can be partitioned recursively, allowing a nested hierarchy to be created. Equal-area cells is the critical criterion, since currently employed equal-angle and constant-area quadrilateral grids can never be equal area and were shown to perform poorly in this respect relative to several alternative grids.

Only two global grids, those based on the triangular partitioning of the Icosahedral Snyder Equal Area (ISEA) projection and partitioning using the Small Circle Subdivision method (not discussed in this article but described in Song 1997) will produce equal-area cells on the spheroid. The Small Circle Subdivision method has the advantage of producing cells slightly more compact, but the ISEA grid is currently more efficient to compute and easier to implement. Consequently, we recommend the ISEA as the best current choice for an equal area global grid. Whichever global grid is selected there are implementation issues that must be addressed in future research, including:

- Implementing an efficient addressing scheme for binning data into grid cells;
- Creating algorithms for fast translation of gridded data to and from geodetic latitude and longitude;
- Developing efficient algorithms for aggregation and disaggregation among nested grid levels; and
- Implementing efficient data storage and access schemes for data in nested cells, including metadata storage and access.

We have begun to address several of these implementation facets for the ISEA grid, beginning with an ETOPO5 DEM dataset binning experiment conducted at several levels of recursion (see <http://bufo.geo.orst.edu/firma/tc/gg> for binning examples). Performing similar implementation experiments on additional datasets using other candidate grids would provide a complementary grid comparison that, together with our geometrical comparisons,

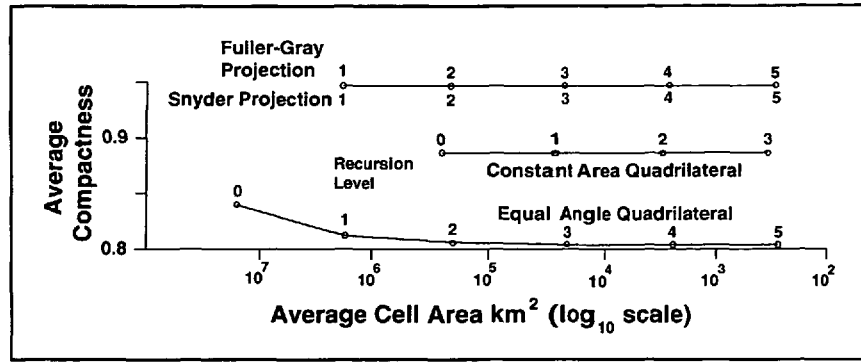


Figure 19. Normalized subcell average compactness vs. average cell area for four global grids.

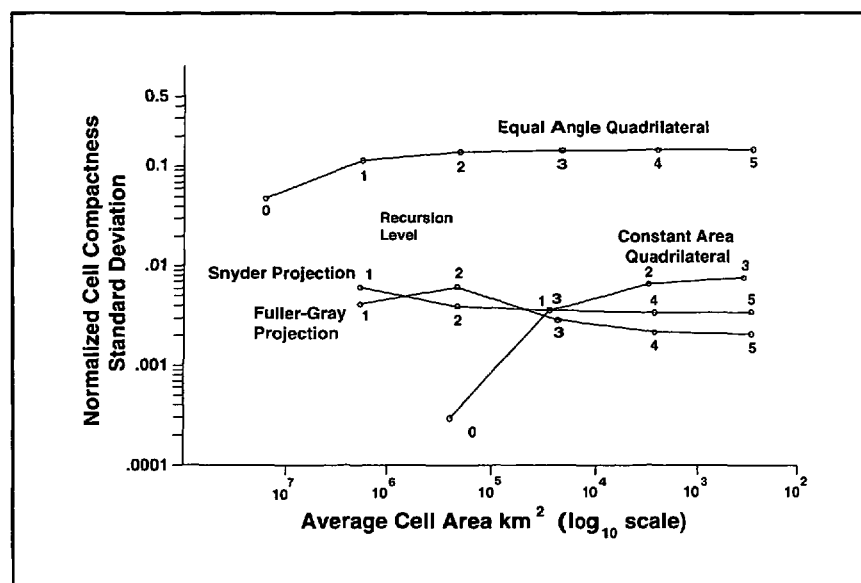


Figure 20. Normalized subcell compactness standard deviation vs. average cell area for four global grids.

will give a full picture of the strengths and weaknesses of current global grid alternatives.

APPENDIX: Zone Standardized Compactness (ZSC) Derivation

The surface area of a spherical zone is computed from:

$$\text{Zone area} = 2 \times \pi \times r^2 (1.0 - \sin \phi) \quad (1)$$

where r is the radius of the sphere and ϕ is the latitude of the bounding parallel.

Setting the zone surface area equal to the cell area, we obtain:

$$\text{Cell area} = 2\pi r^2(1.0 - \sin \phi) \quad (2)$$

so that

$$\sin^2 \phi = \left(1.0 - \frac{\text{cell area}}{2\pi r^2}\right)^2 \quad (3)$$

and

$$\cos \phi = \sqrt{1.0 - \left(1.0 - \frac{\text{cell area}}{2\pi r^2}\right)^2} \quad (4)$$

The perimeter of the spherical zone is the circumference of the bounding parallel, computed from:

$$\text{Zone perimeter} = 2\pi r(\cos \phi) \quad (5)$$

Zone Standardized Compactness (ZSC) is given by Zone perimeter/Cell perimeter. Substituting and combining equations, we compute ZSC from:

$$ZSC = \sqrt{4\pi \times \text{cell area} - \text{cell area}^2/r^2} / \text{cell perimeter} \quad (6)$$

ACKNOWLEDGMENTS

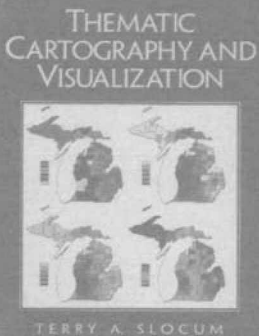
This research was supported by U.S. Environmental Protection Agency—Oregon State University Cooperative Agreement CR 821672. Matthew Gregory, Department of Geosciences graduate student, created the centerpoint distance maps seen in Figure 16. Dr. Ralph Kahn, NASA-JPL, also contributed significantly to this manuscript. This manuscript has been subjected to EPA review and approved for publication. The conclusions and opinions are solely those of the authors and not necessarily the views of the Agency.

REFERENCES

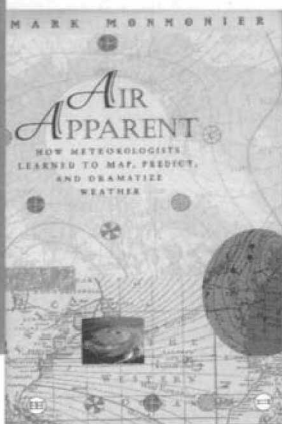
- Baumgardner, J.R., and P.O. Frederickson. 1985. Icosahedral discretization of the two-sphere. *S.I.A.M. Journal of Numerical Analysis* 22(6): 1107-15.
- Bomford, G. 1971. *Geodesy*. Oxford: The Clarendon Press. 731 pp.
- Brooks, D.R. 1981. Grid systems for Earth radiation budget experiment applications. *NASA Technical Memorandum 83233*. 40 pp.
- Coxeter, H.S.M. 1962. The problem of packing a number of equal nonoverlapping circles on a sphere. *Transactions, New York Academy of Science, Division of Mathematics, Series II*, vol. 24: 320-31.
- Dutton, G. 1988. Geodesic modeling of planetary relief. *Cartographica* 21:188-207.
- Dutton, G. 1994. Geographical grid models for environmental monitoring and analysis across the globe (panel session). In: *Proceedings of GIS/LIS '94 Conference*, Phoenix, Arizona.
- Eidenshink, J.C., and J.L. Faundeen. 1994. The 1 km AVHRR global land data set: First stages of implementation. *International Journal of Remote Sensing* 15:3443-62.
- Fekete, G., and L. Treinish. 1990. Sphere quadtree: A new data structure to support the visualization of spherically distributed data. *SPIE: Extracting meaning from complex data: Processing, display, interaction*. Vol. 1259, pp. 242-53.
- Fuller, R.B. 1982. *Synergetics*. New York: MacMillan.
- Giacaglia, G.E.O., and C.A. Lundquist. 1972. Sampling functions for geophysics. *Smithsonian Astrophysical Observatory Special Report No. 344*, 93 pp.
- Goodchild, M.F. 1994. Geographical grid models for environmental monitoring and analysis across the globe (panel session). In: *Proceedings of GIS/LIS '94 Conference*, Phoenix, Arizona.
- Gray, R.W. 1994. Exact transformation equations for Fuller's world map. *Cartography and Geographic Information Systems* 21(4): 243-46.
- Hastings, D.A. 1996. The global land 1-km base elevation digital elevation model: A progress report. *Global Change Newsletter* 27: 11-12.
- Heikes, R., and D.A. Randall. 1995. Numerical integration of the shallow-water equations on a twisted icosahedral grid. Part I: Basic design and results of tests. *Monthly Weather Review* 123:1862-80.
- Kahn, R. 1995. What shall we do with the data we are expecting in 1998? In: *Proceedings of the Massive Data Sets Workshop*, Committee on Applied and Theoretical Statistics, National Academy of Sciences, Washington DC.
- Kimerling, A.J. 1984. Area computation from geodetic coordinates on the spheroid. *Surveying and Mapping* 44(4): 343-51.
- Kimerling, A.J., D. White, K. Sahr, and L. Song. 1995. Development of global sampling grid. *Mid-project report: Sampling design and statistics research for EMAP Program*. U.S. Environmental Protection Agency, Corvallis, Oregon.
- Loveland, T.R., J.W. Merchant, D. O. Ohlen, and J.F. Brown. 1991. Development of a land-cover characteristics database for the conterminous U.S. *Photogrammetric Engineering and Remote Sensing* 57(11): 1453-63.
- Lukatela, H. 1987. Hipparchus geopositioning model: An overview. In: *Proceedings of Auto Carto 8 Symposium*, Baltimore, Maryland, pp. 87-96.
- Maling, D.H. 1992. *Coordinate systems and map projections* (2nd ed.). Oxford, U.K.: Pergamon Press.
- Muehrcke, P.C., and J.O. Muehrcke. 1997. *Map use* (4th ed.). Madison, Wisconsin: JP Publications.
- Olea, R.O. 1984. Sampling design optimization for spatial functions. *Mathematical Geology* 16:369-92.
- Saff, E.B., and A.B.J. Kuijlaars. 1997. Distributing many points on a sphere. *The Mathematical Intelligencer* 19(1): 5-11.
- Slade, G. 1994. Self avoiding walks. *The Mathematical Intelligencer* 16(1):29-35.
- Snyder, J.P. 1987. *Map projections—A working manual*. Washington, DC: U.S. Government Printing Office.
- Snyder, J.P. 1992. An equal-area map projection for polyhedral globes. *Cartographica* 29(1):10-21.
- Song, L. 1997. Small circle subdivision method for development of global sampling grid. Unpublished Masters thesis, Oregon State University, 176 pp.
- Stauffer, D. 1992. *Introduction to percolation theory* (2nd ed.). London, U.K.: Taylor & Francis.
- Tobler, W.R., and Z. Chen. 1986. A quadtree for global information storage. *Geographical Analysis* 18(4): 360-71.
- White, D., A. J. Kimerling, and W.S. Overton. 1992. Cartographic and geometric components of a global sampling design for environmental monitoring. *Cartography and Geographic Information Systems* 19:5-22.
- White, D., A.J. Kimerling, K. Sahr, and L. Song. 1998. Comparing area and shape distortion on polyhedral-based recursive partitions of the sphere. *International Journal of Geographical Information Science* 12: 805-27.
- Wolfram, S. 1986. Cellular automaton fluids 1: Basic theory. *Journal of Statistical Physics* 45:471-526.

Books from ACSM

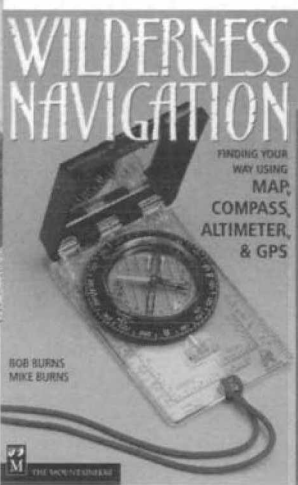
Recently adopted titles
in cartography, GIS,
remote sensing
and GPS



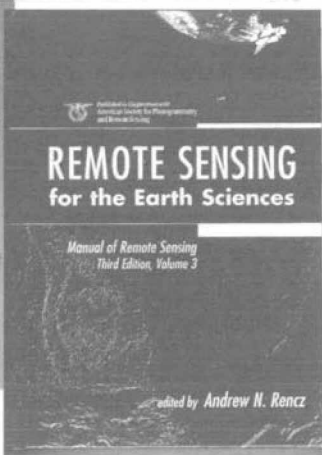
**Thematic Cartography
and Visualization**
Terry A. Slocum



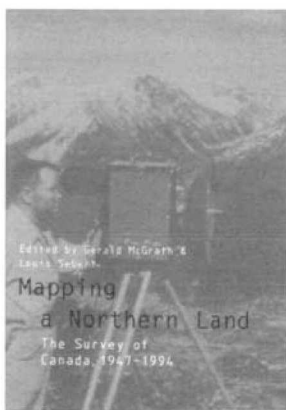
**Air Apparent: How
Meteorologists Learned
to Map, Predict, and
Dramatize Weather**
Mark Monmonier



Wilderness Navigation
Bob and Mike Burns



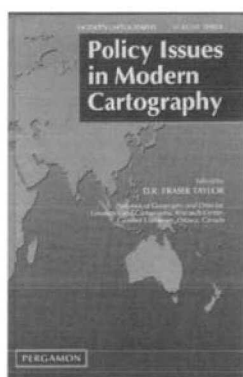
**Remote Sensing for the
Earth Sciences (3rd ed.)**
Andrew Rencz



**Mapping a Northern Land:
The Survey of Canada**
Gerald McGrath and Louis
Sebert (eds.)



Maps with the News
Mark Monmonier



Policy Issues in Modern Cartography
D.R. Frazer Taylor (ed.)

Visit us
on the Web:
www.surveymap.org

Order by Fax
301/493-8245